Applied Energy 327 (2022) 120100

Contents lists available at ScienceDirect

Applied Energy

journal homepage: www.elsevier.com/locate/apenergy

The preload force effect on the thermal runaway and venting behaviors of large-format prismatic $LiFePO_4$ batteries

Zhuangzhuang Jia, Laifeng Song, Wenxin Mei *, Yin Yu, Xiangdong Meng, Kaiqiang Jin, Jinhua Sun, Qingsong Wang *

State Key Laboratory of Fire Science, University of Science and Technology of China, Hefei 230026, PR China

HIGHLIGHTS

- As the preload force increases, the safety vent opens earlier.
- The battery expansion behavior has a mitigating effect on the gas pressure.
- By constructing a TR hazard assessment model, the TR hazard is smallest at 3 kN.

ARTICLE INFO

Keywords:
Lithium-ion battery safety
Preload force
Thermal runaway
Gas venting
Expansion mitigating

ABSTRACT

In electrochemical energy storage systems, large-format $LiFePO_4$ (LFP) batteries are usually formed the battery pack under preload force. However, the preload force effect on the safety of the batteries remains unclear. In this study, the TR and gas venting of the 280 Ah LFP batteries at 100% state of charge under four preload forces (0, 3, 6, and 9 kN) are investigated experimentally. The novelty compared to previous studies is that the fixture with a pressure sensor is used to set different preload forces before the experiment and monitor the expansion behavior of the LFP batteries during TR. The results quantitatively analyse the relationship between preload force and TR hazard of prismatic LFP battery. Two important results are presented: (I) the gas release inside LFP battery is horizontal and vertical at the same time, and the battery expansion behavior has a mitigating effect on gas pressure. (II) the TR hazard assessment model is pioneered to assess the TR hazard of batteries under four preload forces. The results show that the TR hazard is minimal at 3 kN. These results provide an effective guide to the setting of preload force and the emergency response to TR.

1. Introduction

With the global energy crisis and environmental pollution problems becoming increasingly serious, the development and utilization of clean and renewable energy are imperative [1,2]. Electrochemical energy storage (EES) is currently the most widely used and most promising power storage technology [3]. Especially, due to the long lifespan and high energy density [4], lithium-ion batteries (LIBs) occupy the dominant position and have gained popularity in EES systems [5]. Driven by the significant growth of the domestic new energy generation scale and the continuous decline of LIB cost [6], the installed scale of EES has been maintaining a high growth trend. According to incomplete statistics, as of 2021, China's EES scale of operation had reached 1.87 GW, and the cumulative installed capacity reached 5.51 GW, with an increase of 68.5 %. Among them, LIBs have occupied the largest cumulative installation scale.

The preload force, which is the force acting on the entire large surface of the LFP battery, is mainly used to form the large-format batteries into a battery pack in EES [7]. The large-format LFP batteries are charged and discharged under the action of preload force [8]. Some work has been done for the preload force effect on the performance of the battery. Masmoudi et al. [9] documented a coupled mechanical, thermal and chemical model for the electrode particles, which showed that a moderate external pressure caused a longer lifespan of the battery. Kwak et al. [10] analyzed the nonlinear effect of the preload magnitude on the mechanical behavior quantitatively, and showed that the initial slope at low states of charge (SOCs) was significantly dependent on the initial pressure, whereas those at medium and high SOCs were almost the same. In addition to the cycling performance of the LFP battery, the

* Corresponding authors.
E-mail addresses: heart@ustc.edu.cn (W. Mei), pinew@ustc.edu.cn (Q. Wang).

https://doi.org/10.1016/j.apenergy.2022.120100
Received 8 July 2022; Received in revised form 22 September 2022; Accepted 2 October 2022
Available online 14 October 2022
0306-2619/

Nomenclature

Symbols

EES	electrochemical energy storage
LIB	lithium-ion battery
TR	thermal runaway
LFP	$LiFePO_4$
SOC	state of charge
T	temperature (°C)
U	voltage (V)
t	time (s)
M	mass (g)
FED	fractional effective dose
F	force (kN)
P	pressure (Pa)
S	area (m^2)
NCM	$Ni_xCo_yMn_{(1-x-y)}O_2$
FTIR Spectrometer	Fourier Transform Infrared Spectrometer
ρ	density (kg/m^3)
V	volume (L)
v	velocity (m/s)

Subscripts

SV	safety vent
side	the side of the battery
mid	the middle of the battery
down	the bottom of the battery
max	maximum
tr	thermal runaway
ISC	internal short circuit
d	duration
gas	released gas from the battery
print	the value displayed by the balance
b	battery
open	opening of the safety vent

safety performance also plays an important role during the operation of the battery. The thermal runaway (TR), an internal feature of energy carriers, has become a big hindrance to the operation of EES [11]. The TR is a major safety concern for LIB, which is a chemical exothermic reaction accompanied by heat generation and gas release [12,13]. Bai et al. [14] investigated the effect of mechanical extrusion force on the TR of pouch LIBs under overheating, and found that the TR onset occurred faster for higher squeezing pressures, the jet fire duration was shorter, while the flame temperature and area increased. Xian et al. [15] comparatively studied the difference of TR characteristics of the $Ni_{0.8}Co_{0.1}Mn_{0.1}O_2$ battery with or without preload force, and found that the battery combustion process with and without preload force was similar, but the battery combustion was more intense and shorter under the preload force. The study of preload force effect on the battery is mainly focused on pouch $Ni_xCo_yMn_{(1-x-y)}O_2$ (NCM) batteries. There are few studies on the preload force effect on the TR behavior of prismatic LFP batteries. In previous experiments on LFP batteries, the certain preload force is usually applied to the large surface of the LFP battery before the experiment to prevent the battery from over-expansion during TR [16–20]. There is no quantitative analysis of the preload force in previous experiments. The preload force also affects the gas venting of the LFP battery. Huang et al. [21] studied the TR behavior and internal propagation mechanism of the LFP battery under different heating positions, and measured the jet velocity of the LFP battery during TR. They found the jet velocity was much greater under large surface heating mode more than twice that of side heating and bottom heating modes, which may be related to the reaction and the expansion inside the battery. The preliminary conclusion so far is that the physical effects of the preload force on the interior of the battery cause changes in the gas venting velocity [22]. So, there is still a lack of effective research between the preload force and gas venting of LFP battery.

To fill this knowledge gaps and quantify the preload force effect on the TR and gas venting behaviors of large-format prismatic LFP batteries. This study presented the preload force effect on the TR of the large-format LFP battery and the relationship between gas venting velocity and expansion of the battery. Compared with previous studies, the novelty and contribution of the proposed method lie in the following innovative points:

(I) The 280 Ah LFP batteries were tested experimentally by overheating at 0, 3, 6, and 9 kN, where the gas venting velocity, type, temperature and expansion force of the batteries were recorded. Quantitative analysis of the preload force effect on the thermal and gas venting behavior of the LFP battery.

(II) The TR hazard assessment model is pioneered to assess the TR hazard of batteries under four preload forces. The assessment results show that the TR hazard is minimal at 3 kN.

This work fills in the effect of preload force on the TR and gas venting behaviors of the large-format LFP battery and provides a reference value for the minimum hazard preload force by building an evaluation model. This provides an effective theoretical guide for the setting of preload force for LFP batteries and the emergency response of TR.

2. Experimental

2.1. The $LiFePO_4$ battery sample

The battery sample is a commercial LIB that is used in the EES system. The electrodes are $LiFePO_4$ and graphite. The battery case is metal with a plastic wrapper. The nominal capacity and voltage of the battery are 280 Ah and 3.2 V, respectively. The mass and physical dimensions of the LIB are shown in Table 1. Each tested LIB was charged to 100 % SOC by using a battery cycler (NEWARE CT-4004 -30V50A-NFA) at constant current and constant voltage (CC-CV). After charging was completed, the LIB was maintained for 24 h to ensure its stability.

2.2. Experimental apparatus and procedures

This experiment was performed in the combustion chamber, which was fabricated following ISO9705 and ISO5660 [17,23]. The size of the combustion chamber is 1.8 m × 1.8 m × 2 m. The diagram of the combustion chamber is shown in Fig. 1(a). There is a smoke exhaust duct

Table 1
The essential parameters of the tested LFP battery.

Name	Unit	Value
Cathode	–	Lithium phosphate ($LiFePO_4$)
Anode	–	Graphite
Dimension(length × width × height[a])	mm^3	205 × 174 × 72
Safety vent (length × width)	mm^2	31 × 19
Nominal capacity	Ah	280 ± 3.50
Maximum cut-off voltage	V	3.65
Minimum cut-off voltage	V	2.50
Mass	kg	5.42 ± 0.30
State of charge	%	100
Energy density	Wh/kg	165.31

[a] Height does not include the tabs.

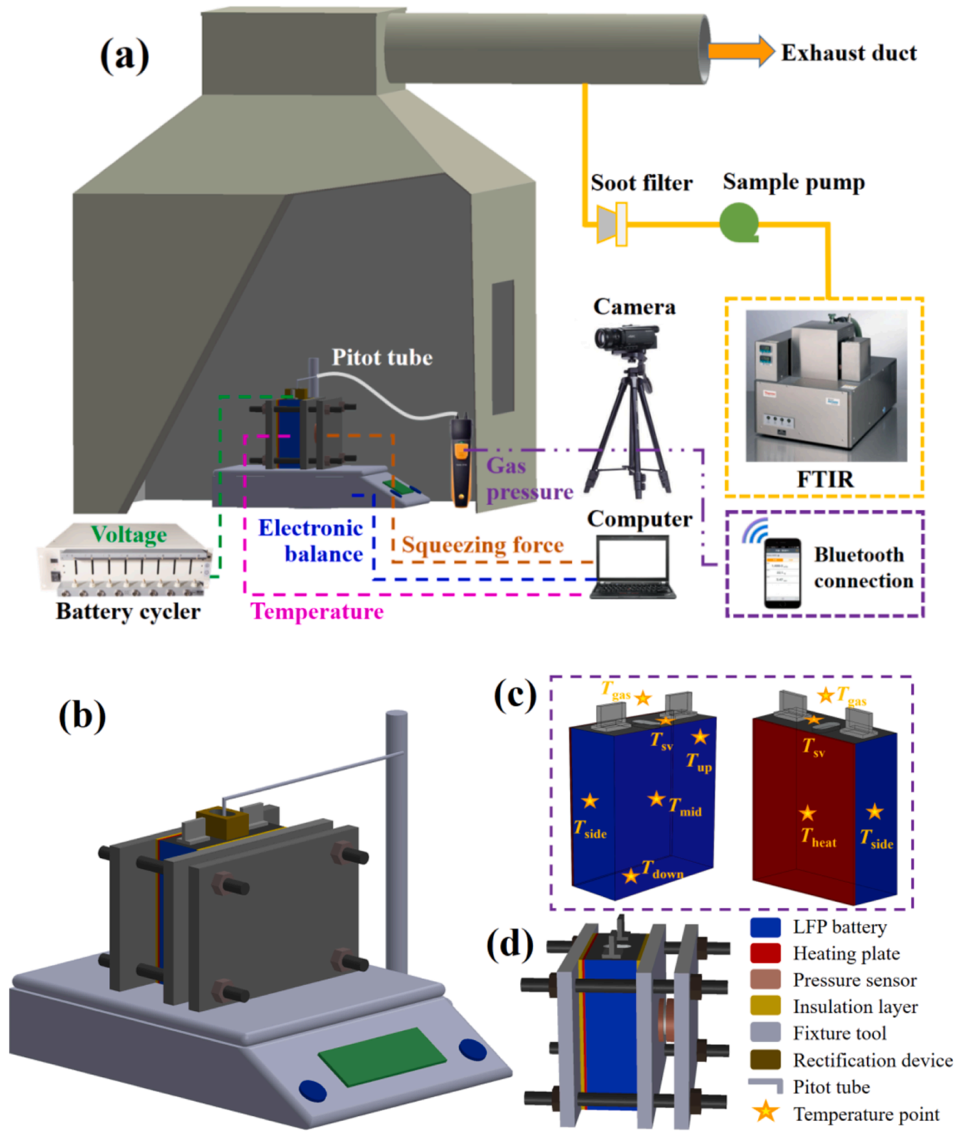

Fig. 1. Experimental overview. (a) Experimental setup. (b) Arrangement of gas release detection device. (c) Arrangement of thermocouple. (d) Diagram of three-page iron fixture tool and pressure sensor.

on the upper side of the combustion chamber, which maintains a constant airflow of 279 L/s during the test. To monitor the composition and content of the gases in real-time, the flow stabilizing blade and the detection are observed in the smoke exhaust duct. A sampling port is set up in the exhaust duct and the sample is extracted from the flue. The sampling data is analyzed by Fourier Transform Infrared Spectrometer (FTIR Spectrometer). The gas concentration during TR can be obtained by the Thermo Scientific™ Antaris™ IGS Gas Analyzer. To quantitatively analyze the preload force and expansion behavior of the battery and the gas venting velocity, this work introduced a three-page iron fixture with a pressure sensor and arranged a rectification device above the safety vent of the battery. As shown in Fig. 1, the tested battery and heating plate are wrapped with thermal insulation cotton. Then, the battery and heating plate are placed in the fixture, which provides 0, 3, 6 and 9 kN preload, by asking the battery manufacturer and referring to the Chinese standard for lithium-ion batteries for power storage (GB/T 36276–2018). Place a self-designed rectification device above the safety vent and tie the device with a wire above the battery to rectify the gas jet during TR. The size of the rectification device is the same as the safety vent, so that all the gas can flow out of the same opening.

During experiment, the tested battery was placed on the Mettler balance in the combustion chamber. The balance data was used to display and record the mass loss of the battery during TR. In addition, the K-type thermocouples with a diameter of 1 mm were attached to the surface of the battery to measure its surface temperature. The Pitot tube and a thermocouple were arranged 4 cm above the safety vent to detect the gas pressure and temperature of the gas jet. The locations of the Pitot tube and thermocouples are shown in Fig. 1. All temperature data were recorded by the data acquisition equipment (ICPCON I-7018). During the test, a video camera (SONY XPS160) was used to monitor TR behavior and the gas injection phenomenon. As the temperature rise rate of the battery surface is > 1 ℃/s, close the heating plate and wait for the battery to cool down, the experiment is finished.

3. Results and discussion

3.1. Thermal runaway characteristics of LFP batteries

Fig. 2 shows the TR behavior of the 280 Ah LFP battery at 0, 3, 6, and 9 kN. According to the TR behavior, the TR phase was divided into 6 stages. At stage I, the LIB was initially heated by the heating plate and the battery behaved all right. At stage II, as the battery was heated for

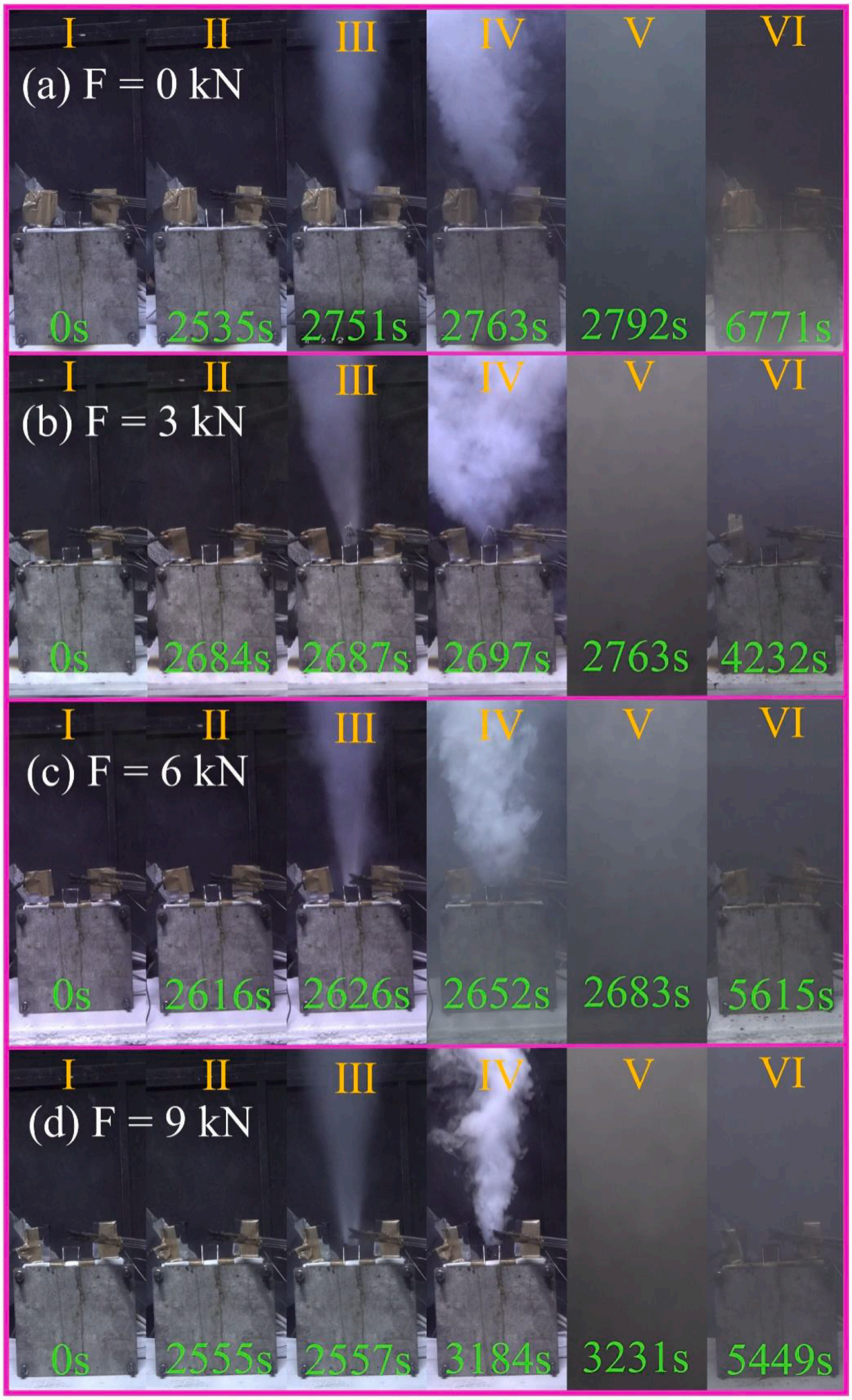

Fig. 2. The thermal runaway behavior of LFP batteries under different preload forces.

longer, the battery temperature gradually increased. The gases were generated due to the redox reaction inside the battery and the electrolyte evaporated at high temperatures, which caused the pressure to increase inside the battery before the safety venting. Especially, as the LFP battery size increases, the LFP battery is more likely to expand. As shown in Fig. 2, the expansion behavior of the battery at this stage was more obvious. At stage III, the safety vent opened and a large jet of electrolytes and gases was released at this stage. As the increase of preload force, the time of the safety venting gradually advanced. The external preload force inhibits the battery expansion, so that the pressure inside the battery is more likely to increase, which leads to the safety venting earlier.

It is interesting for the interval time between the safety venting and the TR at different preload forces at stage IV. At 0, 3, and 6 kN, after the safety venting for 10–26 s, the battery released a large amount of smoke and the TR began to occur. However, at 9 kN, after the safety venting for 627 s, the battery released gas and the TR occurred. Because the safety vent opened early at 9 kN, the internal temperature of the battery was also lower at the moment. Moreover, the battery ejected a large number of electrolytes at the safety venting, and these electrolytes carried away some heat, lowering the temperature inside the battery. So the safety venting early at 9 kN had an inhibiting effect on the TR of the battery. At stage V, the battery began to release a large amount of smoke. Although the combustion chamber had an exhaust port and the exhaust velocity was 279 L/s, the fumes still filled the combustion chamber and the visibility of the combustion chamber was 0. At stage VI, the experiment was finished. The smoke and gases of the combustion chamber gradually disappeared and the interior of the chamber was visible.

3.2. The variation of temperature and voltage

The surface temperature and the voltage of the battery are important for the TR evaluation and early warning of the battery [24,25]. In this work, six thermocouples were arranged on the surface of the battery to detect the temperature variation during TR, respectively. Fig. 3 shows the variation of temperature and voltage with the time under four preload forces. The voltage drop occurred after the TR of the battery, so the voltage of the battery cannot be used as an early warning, which provided a reference for the 280 Ah large-format LFP battery.

Before the TR of the battery, the side temperature of the LFP battery (T_{side}) and the temperature of the safety vent (T_{sv}) are significantly greater than the temperatures at the three temperature points (T_{up}, T_{mid}, and T_{down}) on the back of the battery. Because T_{side} and T_{sv} are heat-conducting by the shell, T_{up}, T_{mid}, and T_{down} are mainly the two internal cells heat-conducting. It can be seen that the internal cells' heat transfer rate is less than the battery shell, and the heat generation of the second cell is smaller, so the T_{up}, T_{mid}, and T_{down} are lower. The temperature difference between the T_{side} and T_{sv} decreases gradually with the increase of the preload force. Because as the preload force increases, the thermal resistance of the contact between the battery and the heating plate decreases, and the battery is heated more evenly.

The gas temperature of the battery is influenced by the preload force, as seen in Fig. 3. The maximum gas temperature values at 0 and 9 kN are significantly higher than at 3 and 6 kN. Moreover, the trend of T_{gas} at 9 kN is different from that of other preload forces. The safety vent opens at 2552 s, the electrolyte and gas are ejected, and T_{gas} rises abruptly to 106 °C at 9 kN. But the battery does not undergo TR, so there is an instantaneous peak in the value. The three temperature points (T_{up}, T_{mid}, and T_{down}) on the surface of the battery are located in the upper, middle and lower parts of the battery. During TR, T_{side} and T_{down} show the highest temperature values of all independent temperature detection points for the batteries. Due to the ejection of the reaction substance at the moment of the safety venting and the evaporation of the electrolyte after the safety venting, the upper and middle parts of the battery have less reactive material. There is less loss of reactive material in the lower part of the battery and more heat is released during TR, so the T_{down} is greater than the T_{up} and T_{mid}. The temperature value of the T_{side} is mainly due to the heat transfer from the heating plate through the battery case and the two cells of the battery during TR. Therefore, the maximum temperature value (T_{max}) of the battery is shown as Eq. (1).

$$T_{max} \in \max\{T_{side\#max}, T_{mid\#max}\} \tag{1}$$

Table 2 shows the key time points and temperature values for the LFP batteries. During TR, T_{SV} is selected as a landmark temperature value

Table 2
Experimental data for the LFP batteries with various preload forces.

Preload force	0 kN	3 kN	6 kN	9 kN
T_{open} (s)	2751 ± 66	2682 ± 54	2623 ± 82	2552 ± 91
t_{tr} (s)	2855 ± 83	2718 ± 69	2652 ± 50	3204 ± 116
t_{ISC} (s)	2994 ± 62	2873 ± 41	2802 ± 77	3293 ± 84
t_d (s)	301 ± 17	275 ± 8	292 ± 12	175 ± 6
T_{open} (°C)	146.9 ± 11.9	144.3 ± 6.3	157.5 ± 9.7	158.1 ± 14.5
T_{tr} (°C)	202.6 ± 16.4	179.5 ± 8.6	185.9 ± 13.1	204.2 ± 10.8
T_{max} (°C)	447.5 ± 17.2	434.1 ± 2.3	425.9 ± 21.4	465.3 ± 12.5

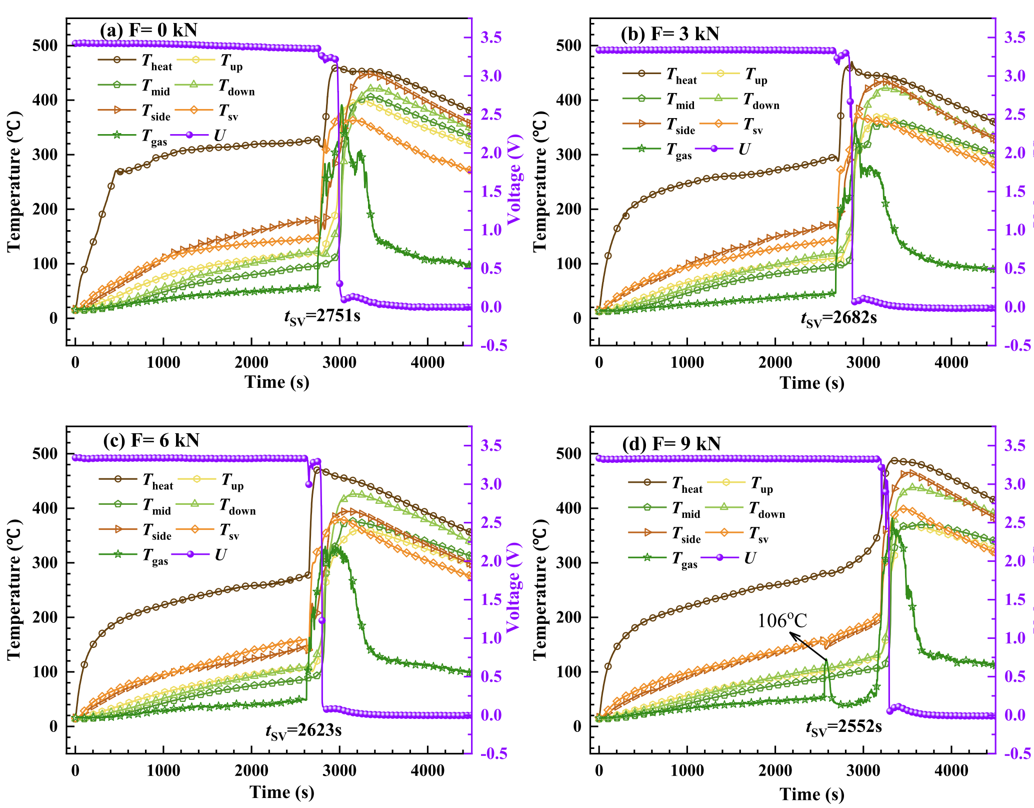

Fig. 3. The variation of temperature and voltage with the time under different preload forces.

based on the principle of arranging temperature detection points in the practical case of EES systems. T_{open} and T_{tr} are strongly influenced by the preload force. At 9 kN, T_{open} and T_{tr} are both maximum values under the four preload forces, which indicates that the battery is less prone to fail at 9 kN. However, T_{open} and T_{tr} are minimum, which indicates that the battery is more susceptible to fail at 3 kN.

Fig. 4 shows the temperature rise rate curve of the T_{sv} during TR. The maximum temperature rise rate of the LFP batteries increases with the increase of the preload force at 0, 3, and 6 kN. With the increase of preload, the contact between electrode and electrolyte is closer and the TR reaction is more intense and heat generation is faster. At 9 kN, the maximum temperature rise rate is 4.2 °C/s, which is mainly due to the volatilization of electrolytes. The electrolyte evaporation leads to the reduction of reactants before the TR, and the rate of heat generation becomes the smallest at the instant of the reaction. So, excessive preload force can cause the safety venting early, which reduces the maximum rate of temperature rise of the LFP battery.

3.3. Effect of preload force on mass loss and mass loss rate

Fig. 5 shows the mass loss and mass loss rate of LFP batteries under four preload forces. The total mass losses of the LFP batteries are 1146.9, 1138.5, 1155.8, and 1174.1 g at 0, 3, 6, and 9 kN, respectively. so it can be assumed that the preload force does not affect the total mass loss of the LFP batteries. However, the rate of mass loss is different at 0, 3, 6, and 9 kN. There are two peaks in the mass loss rate of the battery, which correspond to the TR of two rolled cells. When the preload force is 0 kN, the two peaks in the mass loss rate are significantly smaller than the two peaks under other preload forces. Because the internal positive and negative materials of the battery are not tightly connected due to expansion behavior, the chemical reaction during TR is slower and the rate of mass loss is smaller.

Interestingly, the mass loss and the rate of mass loss can be used to analyze qualitatively the impact force of the safety venting of the battery. When the safety vent opened, the balance showed a positive value at 0 and 9 kN. This value is caused by the reverse force generated by the safety venting, which can analyze the impact force of the safety venting. At 0 and 9 kN, when the battery safety vent opened, the mass loss values were 244.3 and 2419.1 g, and the mass loss rates of the battery were 119.1 and 1208.1 g/s, respectively. However, the mass loss is negative values at 3 and 6 kN, and the mass loss rate is also negative values at 3 kN. So the order of impact force of the batteries under four preload forces is 9 kN > 0 kN > 6 kN > 3 kN.

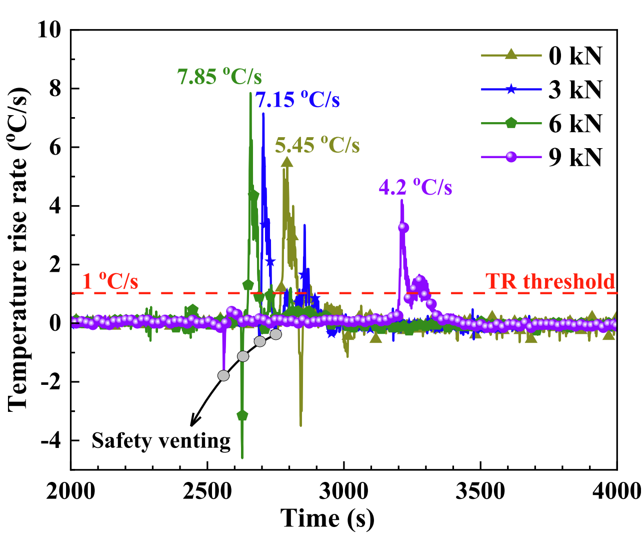

Fig. 4. The temperature rise rate curve of the T_{sv} under four preload forces.

3.4. Expansion performance analysis of LFP battery during thermal runaway

Fig. 6 shows the expansion behavior and gas pressure with the time under four preload forces. After the heating plate starts to heat up, the preload force first decreases, then gradually reaches a stable value at 3, 6 and 9 kN. The preload force rises and then decreases and finally tends to a stable value at 0 kN. Because the insulation wool is crumpled by heat and the heating plate also undergoes thermal expansion during the initial heating of the heating plate, which causes the preload to fluctuate. After the preload is stabilized, due to battery expansion behavior, the expansion force gradually increases until the safety venting. The maximum expansion force of the LFP battery varies at different preload forces.

During TR, there are two peaks of the battery expansion force, which correspond to the peaks of the gas pressure. This shows the gas release is horizontal and vertical at the same time in the process of gas release. At 0 and 9 kN, the maximum gas pressures of the battery are 152 and 170 Pa. This is much larger than the maximum gas pressures at 3 and 6 kN, which are 109 and 116 Pa. This is mainly related to the expansion behavior of the LFP battery. At 0 kN, when the battery itself has reached the maximum expansion and can't occur lateral expansion, the pressure inside the battery can be released through the safety venting. At 9 kN, the preload force acting on the battery is too large, and there is no way to continue to expand laterally during TR, which leads to greater impact pressure of the gas release. However, at 3 and 6 kN, the batteries undergo some internal pressure relief from lateral expansion during TR, which leads to a reduction in gas pressure. The expansion behavior under different preload forces has an important effect on the gas release of LFP batteries.

3.5. Analysis of gas release

3.5.1. Gas release composition and toxicity assessment

The release of typical gases is a key risk factor in the TR process. During thermal abuse, gases may come from the evaporation of organic solvents, thermal decomposition, and chemical reactions among compounds inside the battery [26,27]. So the reactions and gas composition inside the battery are very complex. The composition and volume of gases released from the TR of the battery were precisely measured by FTIR Spectrometer instrumentation. Fig. 7(a-d) shows the real-time gas release of the LFP battery. The peak concentration of the released gas increases with the increase of the preload force during TR. By integrating the gas components, each gas generation and the ratio of each gas component can be obtained. As shown in Fig. 7(e-f), among the measured gas release components, the CO_2 and CO account for the largest ratio of total gas volume. At 6 and 9 kN, the volume of CO_2 gas may reach about 500 and 502 L, which is much larger than the volume of CO_2 gas at 0 and 3 kN. It can be concluded that the order of the measured gas composition percentage of the LFP battery under four preload forces is $CO_2 > CO > CH_4 > C_2H_4 > HCl$. The preload force has little effect on the gas composition percentage.

The total gas release can be found by integrating the gas composition of the LFP battery. As shown in Fig. 7(g), the total volume of gas release at 9 kN is 1009.1 L at maximum. And the total volume of gas release at 6 kN is 966 L, accounting for 95.7 % of the maximum gas release. At 0 and 3 kN, the volumes of gas release are 558 and 524.7 L, accounting for 55.3 % and 52 % of the maximum gas release, respectively. This is mainly due to the earlier safety venting of the battery. A large amount of oxygen reacts with the active material inside the battery to release more carbon dioxide [28], especially, the safety vent opens earlier and a large amount of oxygen enters the battery for reactions after the safety venting at 9 kN.

To evaluate and compare the toxicity of ejected gases under four preload forces, the toxic-gas model described in an international standard (ISO 13571) is employed [29]. It is a good way to quantitatively

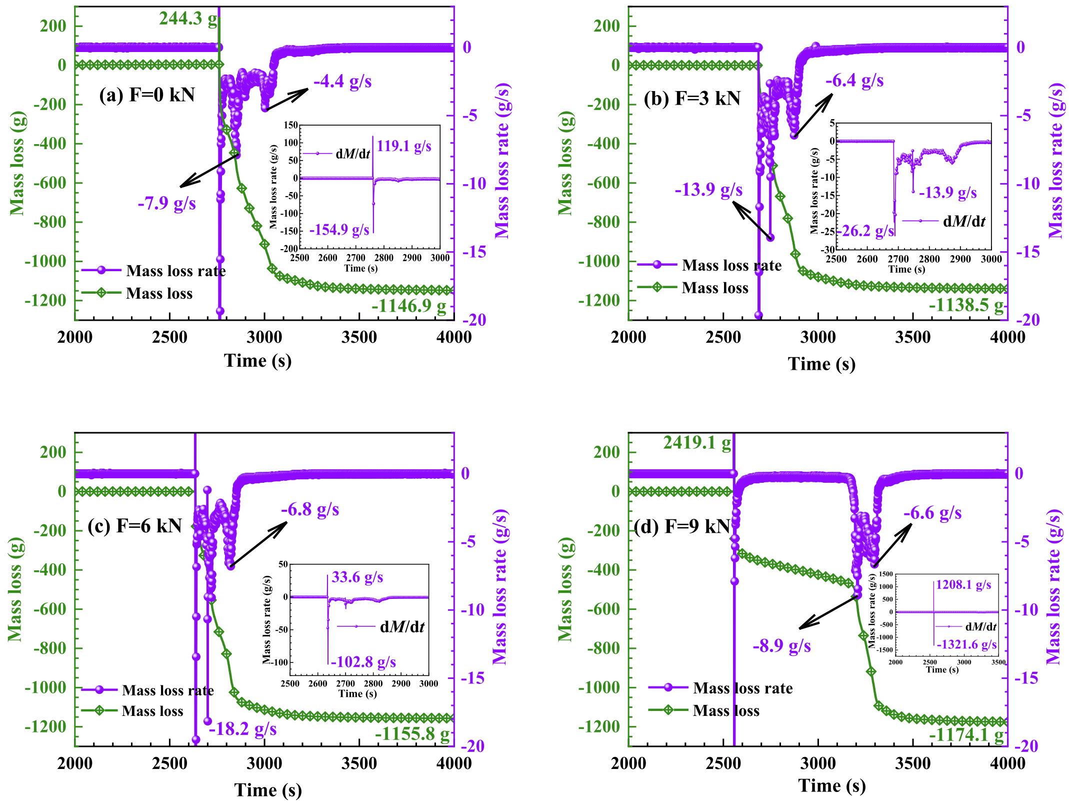

Fig. 5. Mass loss and mass loss rate of LFP batteries under four preload forces.

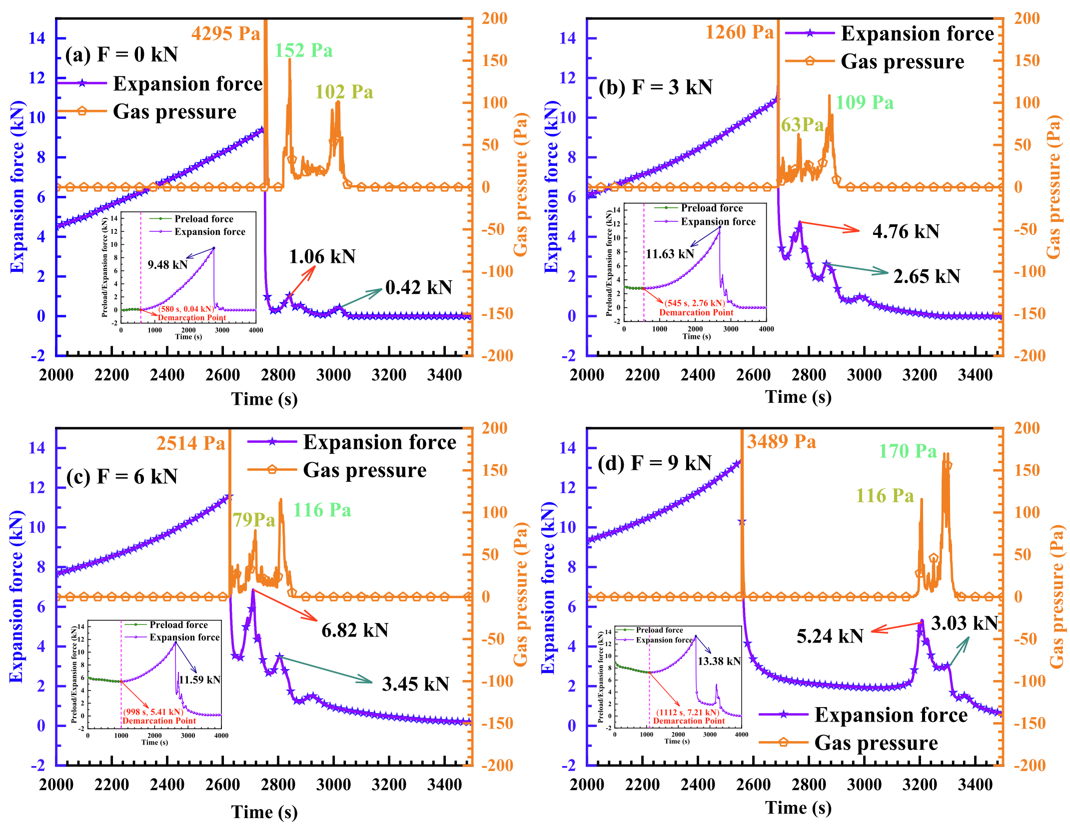

Fig. 6. The expansion force and gas pressure with the time under different preload forces.

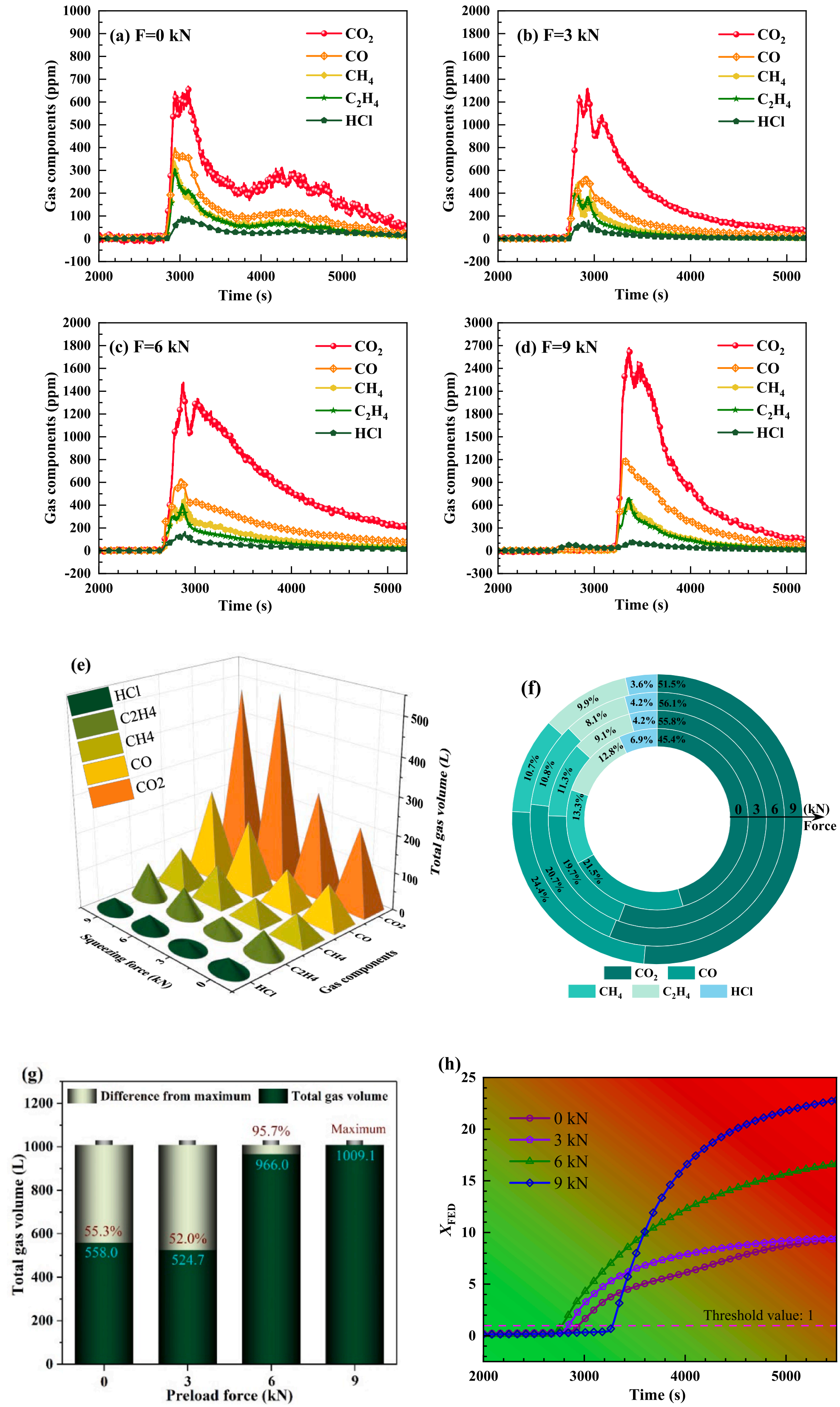

Fig. 7. Analysis of released gas from LFP batteries during TR under four preload forces. (a-d) Variation of gas composition with the time. (e) The total gas volume of CO_2, CO, CH_4, C_2H_4, and HCl. (f) Gas composition percentage of CO_2, CO, CH_4, C_2H_4, and HCl. (g) Total released gases volume from LFP batteries. (h) Assessment of the asphyxiant gases during TR.

assess the overall gas toxicity and has been widely used to evaluate the LIB fire toxicity [30]. In this method, asphyxiation is a key parameter, whose effect can be evaluated by determining the fractional effective dose (FED) calculated by Eqs. (2–3). X_{FED} is the critical concentration of each irritant gas that is expected to seriously compromise occupants' tenability, which is provided by standard ISO 13571.

$$X_{FED} = \sum_{t_1}^{t_2} \frac{v_{co_2}\phi_{co}}{35000}\Delta t + \sum_{t_1}^{t_2} \frac{(v_{co_2}\phi_{HCN})^{2.36}}{1.2\times 10^6}\Delta t \tag{2}$$

$$v_{CO_2} = \exp([CO_2]/5) \tag{3}$$

where ϕ is the concentration of each gas (ppm), $[CO_2]$ is the average volume percent of CO_2. When X_{FED} reaches 1, it means 50 % of the population would be expected to be unable to perform cognitive and motor-skill functions at an acceptable level. As shown in Fig. 7(h), the X_{FED} values are equal at 0 and 3 kN, which is 9.37. However, at 6 and 9 kN, the X_{FED} values are 16.27 and 22.72, respectively. These are much higher than the threshold values, so the toxicity of the gas release during TR is serious under four preload forces. Some ventilation measures should be introduced to reduce gas hazards during the TR of the battery.

3.5.2. Gas venting velocity

The gas venting velocity is an important parameter for the TR behavior of the LFP battery, mainly in terms of battery fire and gas diffusion[31]. An accurate understanding the gas venting velocity is important for battery fire behavior and gas detection. When the LFP battery is heated, the internal pressure of the battery gradually increases with the chemical reactions inside the battery and the volatilization of the electrolyte until the safety venting. For the 280 Ah LFP battery, the critical pressure of the safety venting is set as 0.85 ± 0.2 MPa by consulting the battery manufacturer. In previous studies, the velocity of gas release is usually obtained by the rate of mass loss [32], but the density of the battery and the impact force is not known, so it is not accurate to measure the gas venting velocity. To obtain the gas venting velocity more accurately, we used a method of coupling the Pitot tube and balance measurement. The Pitot tube is a classic velocity measurement tool. As seen in section 3.3, it should also be noted that gas venting is overweight from the mass balance. To analyze the effect of impact, the force analysis was performed on the interface between the battery measurement system and the mass balance. The force balance is shown in Fig. 8.

For the single battery, the analysis of the forces on the battery during TR.

$$F_{gas} = F_{bot} \tag{4}$$

$$P_{gas}S_{vent} = F_{gas} \tag{5}$$

For the balance & battery system, the analysis of the forces on the battery during TR [33].

$$M_{print}g = -M_{loss}g + F_{bot} \tag{6}$$

By integrating Eq.(4), Eq. (5), and Eq. (6), Eq. (7) can be obtained.

$$M_{print}g = -M_{loss}g + P_{gas}S_{vent} \tag{7}$$

$$S_{vent} = \frac{\pi ab}{4} \tag{8}$$

where a and b are the length of the long axis and the length of the short axis in the ellipse (m), respectively. S_{vent} is the area of the safety vent, which is found by Eq. (8), $S_{vent} = 4.62 \times 10^{-4}$ m^2, P_{gas} is the pressure of the gas released from the battery (Pa). As the S_{vent} is very small, the F_{gas} can be ignored, so Eq. (7) can be simplified to Eq. (9).

$$M_{print}g = -M_{loss}g \tag{9}$$

According to the mass conservation equation, Eq. (10) can be obtained.

$$\frac{dM_{loss}}{dt} = \rho S_{vent}v_{gas} \tag{10}$$

By integrating Eq. (9) and Eq. (10), Eq. (11) can be obtained.

$$\frac{dM_{print}}{dt} = -\rho S_{vent}v_{gas} \tag{11}$$

where M_{print} is the value displayed on the balance (g), ρ is the density of the released gases from the battery (kg/m^3), and v_{gas} is the velocity of gas release (m/s).

The P_{gas} is measured by the Pitot tube during TR. According to the empirical equation of Pitot tube measurement can be obtained [5].

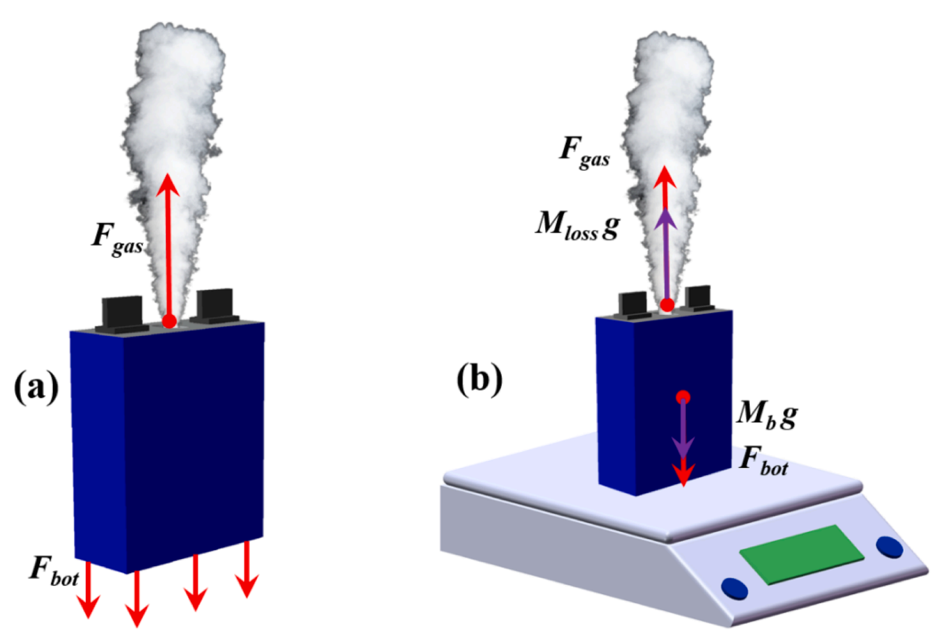

Fig. 8. The analytical diagram of the forces during the gas release of the LIB. (a) The force analysis diagram for a single cell. (b) The force analysis diagram of the system, including battery and balance.

$$v_{gas} = \varepsilon\sqrt{\frac{2P_{gas}}{\rho}} \tag{12}$$

According to the Pitot tube model, it can be derived that the coefficient ε in the empirical equation is 1. The velocity of gas release from the battery can be obtained by integrating Eqs. (10–12), as shown in Eq. (13).

$$v_{gas} = \frac{2P_{gas}S_{vent}}{-\frac{dM_{print}}{dt}} \tag{13}$$

The gas venting velocity under four preload forces can be obtained from the above analysis, as shown in Fig. 9. The duration of gas release for the LFP battery is different under four preload forces. At 0 kN, the time of gas release is the longest. But the time is the shortest at 9 kN. There are two main reasons. (i) During the experiment, the preload force increases, and the contact thermal resistance between the battery and the heating plate becomes smaller. The heat transfer efficiency is higher with the increase of preload force, and the redox reaction inside the battery is more violent, so the TR duration is reduced. (ii) At 0,3 and 6 kN, the TR occurs after the safety venting. However, the TR occurs after the safety venting for 536 s at 9 kN. Before the TR, a large amount of electrolyte evaporates by the vent, the reaction material is reduced, and the reaction time is greatly shortened.

During TR, the gas venting velocity of the batteries appears two peaks under four preload forces, which is caused by the two rolled cells of the LFP battery. Moreover, the maximum gas venting velocity is influenced by the preload force. The maximum gas venting velocities are 32.5 m/s and 31.3 m/s at 0 and 9kN, respectively. However, at 3 and 6 kN, the maximum velocities are only 22.5 and 28.5 m/s, which are mainly influenced by the redox reaction inside the battery and the lateral expansion of the LFP battery. At 0 kN, the preload force is less constrained on the LFP battery, the battery expansion is large. So the safety vent opens when the battery expansion reaches the extreme. At 9 kN, the external preload force is large, the battery expansion is extremely small. During TR, the lateral expansions are very small at 0 and 9 kN, so the gas venting velocities are larger.

3.6. Error analysis and hazard evaluation

3.6.1. Error analysis

To illustrate the reliability of the experimental results, three identical batteries for each experimental condition were adapted as experimental samples. The average values and standard deviations of these key parameters are shown in Fig. 10. It can be seen that the standard deviations of these measured parameters such as T_{max}, t_{SV} and M_{loss} are less than 5 %, which has high data reliability. In addition, the calculated gas venting velocities are well reproduced during the gas venting process. It can be seen that the maximum velocity under the four preload forces is about 23.3–39.1 m/s, and the maximum standard deviation is less than 15 %.

3.6.2. Evaluation of thermal runaway hazard severity

The 280 Ah LFP battery has large hazards to the surrounding environment and people in the TR process. For the LFP batteries, the typical TR behavior is the safety venting, heat generation and gas release. The TR hazard characteristics under four preload forces are evaluated in terms of thermal hazard, explosion hazards, toxic gas hazard and impact hazard. In this paper, from the safety assessment perspective, a qualitative hazard assessment of the TR hazard was developed. According to the type of accident and the severity of the hazard, six main reference values were selected for the assessment model, which are the duration of the TR, the maximum value of the surface temperature of the battery,

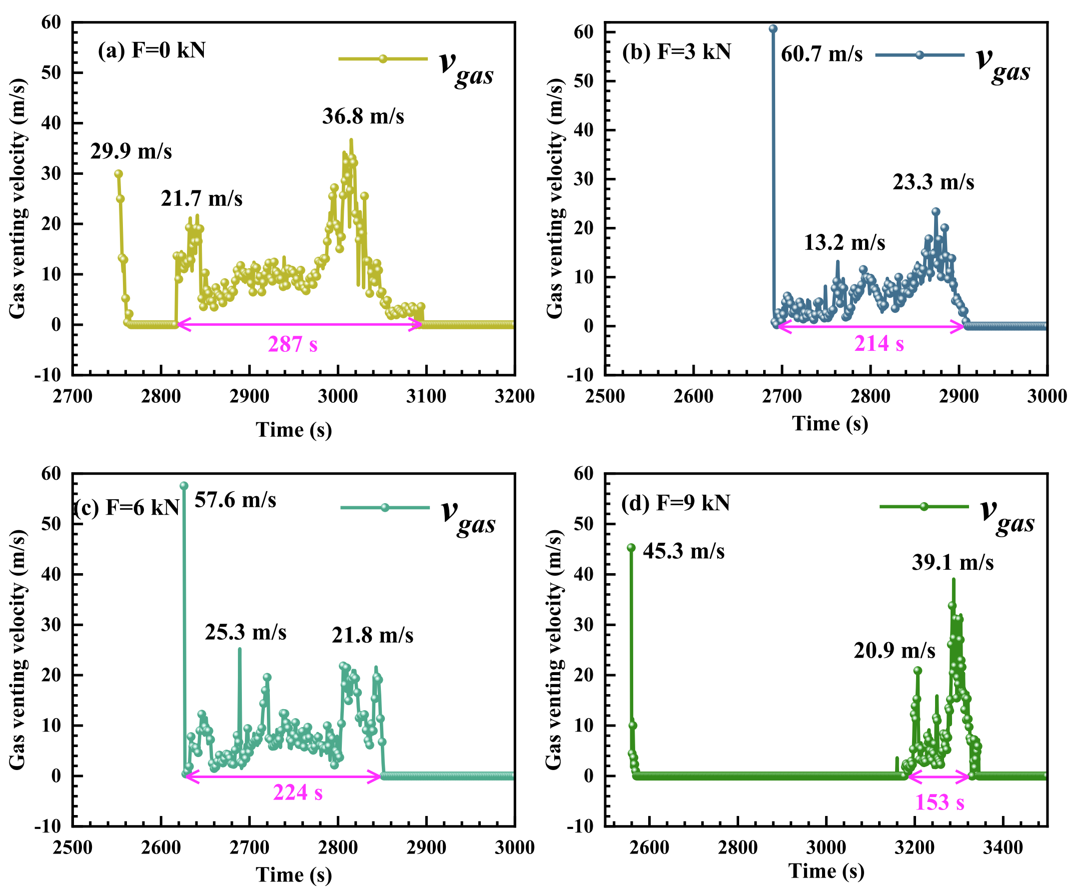

Fig. 9. Variation of the gas venting velocity of LFP batteries during thermal runaway under four preload forces.

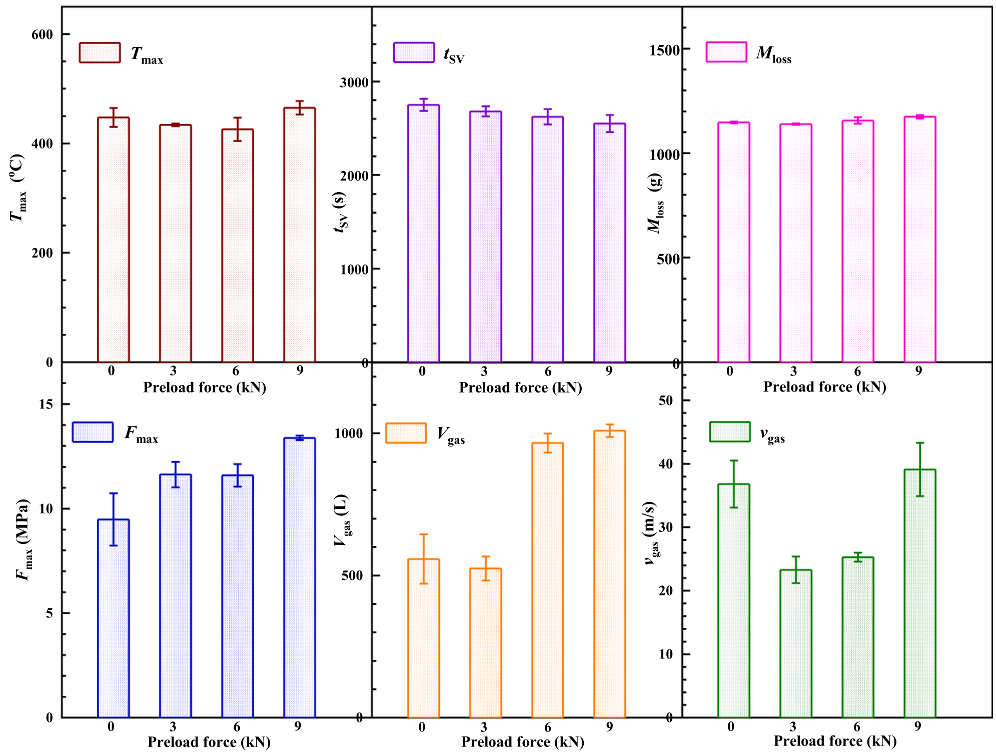

Fig. 10. The error bars of the key parameters.

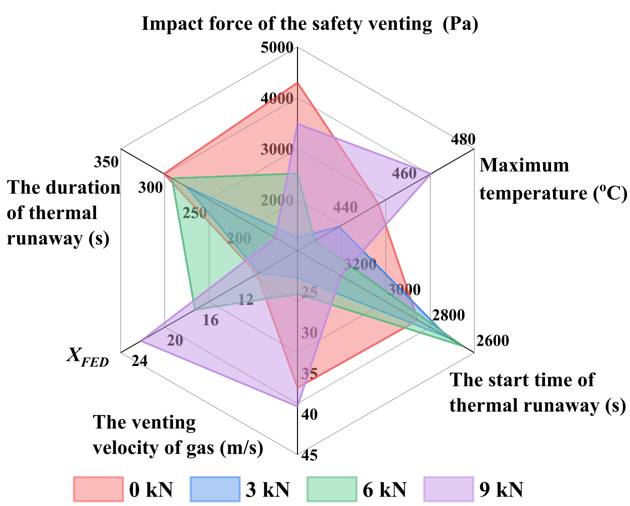

Fig. 11. Comparative assessment of thermal runaway hazards of LFP batteries under different preload forces.

the beginning time of the TR, the maximum gas venting velocity, and the impact force of the safety venting and the FED.

The evaluation model data is shown in Fig. 11, the X_{FED} value and the start time of TR are small during TR at 0 kN, but the other evaluation indexes are relatively large. The impact force and the duration of TR have reached the maximum value, which is more serious for the TR hazard. At 3 and 6 kN, the TR hazard is mainly reflected in the time, the start time of TR and the duration time of TR are large. At 6 kN, the X_{FED} value is also higher in terms of gas release, which is dangerous. Conversely, the duration of TR and the start time of TR are the smallest at 9 kN. But the other indicators are extremely dangerous at 9 kN, the gas venting velocity and X_{FED} value have reached the maximum value. Considering together, the TR hazard of the 280 Ah LFP battery is the smallest at 3 kN, and the TR hazards are the largest at 0 and 9 kN.

4. Conclusions

This paper presents the pioneering study on the TR and venting behaviors of LFP batteries under different preload forces. The experiments were conducted on 280 Ah LFP batteries triggered by overheating, and some behavioral manifestations of the batteries were monitored. The conclusions drawn from this study are listed as follows.

(1)The preload force has a great effect on the safety venting and the TR time. As the preload force increases, the safety vent opens earlier. At 0, 3 and 6 kN, the TR of the LFP battery occurs after the safety venting, and the TR is advanced with the increase of preload force. At 9 kN, the TR occurs at 536 s after the safety venting due to excessive preload force.

(2)The 280 Ah LFP battery has two peaks of expansion force during TR, and the expansion peaks correspond to the peaks of gas pressure from the battery. The gas release of the LFP battery is horizontal and vertical at the same time, and the battery expansion behavior has a mitigating effect on gas pressure. At 0 and 9 kN, the expansion behaviors of the LFP battery are smaller during TR. The mitigation of the gas pressure is small, and the gas venting pressure is large.

(3)By analyzing the gas composition and venting velocity of the battery during TR, the order of the measured gas composition percentage of the LFP battery under four preload forces is CO_2 > CO > CH_4 > C_2H_4 > HCl. The preload force has little effect on the gas composition percentage. However, the total gas volumes at 6 and 9 kN are twice as much as the total gas volumes at 0 and 3 kN. Similarly, the maximum gas venting velocities at 0 and 9 kN are much greater than the maximum gas venting velocities at 3 and 6 kN. The preload force has a significant effect on the total gas volume and the maximum gas venting velocity of the LFP battery.

(4)The TR hazard assessment model is constructed. By comparing the TR hazard of the 280 Ah LFP batteries under four preload forces, it is concluded that the TR hazard is the smallest at 3 kN, and the TR hazards are the largest at 0 and 9 kN.

CRediT authorship contribution statement

Zhuangzhuang Jia: Investigation, Writing – original draft, Formal analysis, Writing – review & editing. **Laifeng Song:** Data curation. **Wenxin Mei:** Visualization, Methodology, Validation. **Yin Yu:** Investigation, Software. **Xiangdong Meng:** . **Kaiqiang Jin:** Writing – review & editing. **Jinhua Sun:** Supervision, Methodology. **Qingsong Wang:** Conceptualization, Supervision, Funding acquisition, Project administration.

Declaration of Competing Interest

The authors declare that they have no known competing financial interests or personal relationships that could have appeared to influence the work reported in this paper.

Data availability

The data that has been used is confidential.

Acknowledgments

This work is supported by the National Key R&D Program of China (No. 2021YFB2402001), the Fundamental Research Funds for the Central Universities (WK2320000051), the China National Postdoctoral Program for Innovative Talents (No. BX20220286) and the China Postdoctoral Science Foundation (No. 2022T150615). Prof. Q.S Wang is supported by Youth Innovation Promotion Association CAS (No. Y201768).

References

[1] Lyu P, Liu X, Qu J, Zhao J, Huo Y, Qu Z, et al. Recent advances of thermal safety of lithium ion battery for energy storage. Energy Storage Mater 2020;31:195–220.

[2] Wang F, Harindintwali JD, Yuan Z, Wang M, Wang F, Li S, et al. Technologies and perspectives for achieving carbon neutrality. The Innovation 2021;2(4):100180.

[3] Wang Y, Sun Y, Zhang Y, Chen X, Shen H, Liu Y, et al. Optimal modeling and analysis of microgrid lithium iron phosphate battery energy storage system under different power supply states. J Power Sources 2022;521:230931.

[4] Jia Z, Huang Z, Zhai H, Qin P, Zhang Y, Li Y, et al. Experimental investigation on thermal runaway propagation of 18,650 lithium-ion battery modules with two cathode materials at low pressure. Energy 2022;251:123925.

[5] Qin P, Jia Z, Wu J, Jin K, Duan Q, Jiang L, et al. The thermal runaway analysis on LiFePO4 electrical energy storage packs with different venting areas and void volumes. Appl Energy 2022;313:118767.

[6] Choi D, Shamim N, Crawford A, Huang Q, Vartanian CK, Viswanathan VV, et al. Li-ion battery technology for grid application. J Power Sources 2021;511:230419.

[7] Oh K-Y, Epureanu BI. Characterization and modeling of the thermal mechanics of lithium-ion battery cells. Appl Energy 2016;178:633–46. https://doi.org/10.1016/j.apenergy.2016.06.069.

[8] Mei W, Duan Q, Lu W, Sun J, Wang Q. An investigation on expansion behavior of lithium ion battery based on the thermal-mechanical coupling model. J Cleaner Prod 2020;274:122643. https://doi.org/10.1016/j.jclepro.2020.122643.

[9] Masmoudi M, Moumni Z, Bidault F. Analysis of the Thermo-Mechanical-Chemical Coupled Response of a Lithium-Ion Battery Particle during a Charge-Discharge Cycle. J Electrochem Soc 2019;166(3):A5445–61. https://doi.org/10.1149/2.0631903jes.

[10] Kwak E, Son DS, Jeong S, Oh K-Y. Characterization of the mechanical responses of a LiFePO4 battery under different operating conditions. J Storage Mater 2020;28:101269. https://doi.org/10.1016/j.est.2020.101269.

[11] Weng J, Yang X, Ouyang D, Chen M, Zhang G, Wang J. Comparative study on the transversal/lengthwise thermal failure propagation and heating position effect of lithium-ion batteries. Appl Energy 2019;255:113761. https://doi.org/10.1016/j.apenergy.2019.113761.

[12] Liu J, Huang Z, Sun J, Wang Q. Heat generation and thermal runaway of lithium-ion battery induced by slight overcharging cycling. J Power Sources 2022;526:231136. https://doi.org/10.1016/j.jpowsour.2022.231136.

[13] Wang Q, Jiang L, Yu Y, Sun J. Progress of enhancing the safety of lithium ion battery from the electrolyte aspect. Nano Energy 2019;55:93–114. https://doi.org/10.1016/j.nanoen.2018.10.035.

[14] Bai J, Wang Z, Gao T, Bai W, Wang J. Effect of mechanical extrusion force on thermal runaway of lithium-ion batteries caused by flat heating. J Power Sources 2021;507:230305. https://doi.org/10.1016/j.jpowsour.2021.230305.

[15] Xian X, Dong H, Zhang S, Li Y, Sheng Y. Effect of clamping force on thermal runaway characteristics of soft-packed NCM lithium-ion power battery. Chinese. J Power Sources 2020;44(05). pp. 682–5+705.

[16] Wang C-J, Zhu Y-l, Gao F, Qi C, Zhao P-L, Meng Q-F, et al. Thermal runaway behavior and features of LiFePO4 /graphite aged batteries under overcharge. Int J Energy Res 2020;44(7):5477–87.

[17] Mao B, Liu C, Yang K, Li S, Liu P, Zhang M, et al. Thermal runaway and fire behaviors of a 300 Ah lithium ion battery with LiFePO4 as cathode. Renew Sustain Energy Rev 2021;139:110717.

[18] Li L, Xu C, Chang R, Yang C, Jia C, Wang Li, et al. Thermal-responsive, super-strong, ultrathin firewalls for quenching thermal runaway in high-energy battery modules. Energy Storage Mater 2021;40:329–36.

[19] Huang Z, Shen T, Jin K, Sun J, Wang Q. Heating power effect on the thermal runaway characteristics of large-format lithium ion battery with Li(Ni1/3Co1/3Mn1/3)O2 as cathode. Energy 2022;239:121885. https://doi.org/10.1016/j.energy.2021.121885.

[20] Huang Z, Liu J, Zhai H, Wang Q. Experimental investigation on the characteristics of thermal runaway and its propagation of large-format lithium ion batteries under overcharging and overheating conditions. Energy 2021;233:121103. https://doi.org/10.1016/j.energy.2021.121103.

[21] Huang Z, Yu Y, Duan Q, Qin P, Sun J, Wang Q. Heating position effect on internal thermal runaway propagation in large-format lithium iron phosphate battery. Appl Energy 2022;325:119778.

[22] Jia Z, Qin P, Li Z, Wei Z, Jin K, Jiang L, et al. Analysis of gas release during the process of thermal runaway of lithium-ion batteries with three different cathode materials. J Storage Mater 2022;50:104302.

[23] Wang Z, Yang H, Li Y, Wang G, Wang J. Thermal runaway and fire behaviors of large-scale lithium ion batteries with different heating methods. J Hazard Mater 2019;379:120730. https://doi.org/10.1016/j.jhazmat.2019.06.007.

[24] Jin Y, Zheng Z, Wei D, Jiang X, Lu H, Sun L, et al. Detection of Micro-Scale Li Dendrite via H2 Gas Capture for Early Safety Warning. Joule 2020;4(8):1714–29.

[25] Ren D, Feng X, Lu L, He X, Ouyang M. Overcharge behaviors and failure mechanism of lithium-ion batteries under different test conditions. Appl Energy 2019;250:323–32. https://doi.org/10.1016/j.apenergy.2019.05.015.

[26] Golubkov AW, Fuchs D, Wagner J, Wiltsche H, Stangl C, Fauler G, et al. Thermal-runaway experiments on consumer Li-ion batteries with metal-oxide and olivin-type cathodes. RSC Adv 2014;4(7):3633–42.

[27] Liao Z, Zhang S, Zhao Y, Qiu Z, Li K, Han D, et al. Experimental evaluation of thermolysis-driven gas emissions from LiPF6-carbonate electrolyte used in lithium-ion batteries. Journal of Energy Chemistry 2020;49:124–35.

[28] Weng J, Ouyang D, Liu Y, Chen M, Li Y, Huang X, et al. Alleviation on battery thermal runaway propagation: Effects of oxygen level and dilution gas. J Power Sources 2021;509:230340.

[29] Huang Z, Li X, Wang Q, Duan Q, Li Y, Li L, et al. Experimental investigation on thermal runaway propagation of large format lithium ion battery modules with two cathodes. Int J Heat Mass Transf 2021;172:121077.

[30] Peng Y, Yang L, Ju X, Liao B, Ye K, Li L, et al. A comprehensive investigation on the thermal and toxic hazards of large format lithium-ion batteries with LiFePO4 cathode. J Hazard Mater 2020;381:120916.

[31] Mao B, Zhao C, Chen H, Wang Q, Sun J. Experimental and modeling analysis of jet flow and fire dynamics of 18650-type lithium-ion battery. Appl Energy 2021;281:116054. https://doi.org/10.1016/j.apenergy.2020.116054.

[32] Zhou Z, Ju X, Zhou X, Yang L, Cao B. A comprehensive study on the impact of heating position on thermal runaway of prismatic lithium-ion batteries. J Power Sources 2022;520:230919. https://doi.org/10.1016/j.jpowsour.2021.230919.

[33] Zou K, Chen X, Ding Z, Gu J, Lu S. Jet behavior of prismatic lithium-ion batteries during thermal runaway. Appl Therm Eng 2020;179:115745. https://doi.org/10.1016/j.applthermaleng.2020.115745.